



Single Image Integrated Deblurring Algorithm in Non-Uniform Environment

Rechard Lee^{1,*}, Celine Wong¹

¹ Mathematics Visualization Research Group, Faculty of Science and Natural Resources, Universiti Malaysia Sabah, Jalan UMS, 88400 Kota Kinabalu, Sabah, Malaysia

ARTICLE INFO

Article history:

Received 25 September 2023

Received in revised form 8 November 2023

Accepted 11 April 2024

Available online 12 May 2024

Keywords:

Blind image deblurring; L_0 -regularized intensity; Gradient prior; Scale aware smoothing; Blur kernels

ABSTRACT

Motion blurriness in an image caused by camera shake during exposure is unavoidable. It could lead to information loss and degradation in the image quality. Therefore, many researchers are dedicated to developing image deblurring techniques to recover clear images from blurred images. During the deblurring process, structural edges in images play a vital part in estimating the blur kernels. For images with rich textures, fine-scale edges become more apparent. This will cause vagueness in the image's structural edges and affect the accuracy of the kernel estimation process. In this study, we propose a single-image motion deblurring by kernel estimation method combined with L_0 -Regularized Intensity and Gradient Prior, and enhanced Scale Aware Smoothing methods. Two types of non-uniform datasets are used, which are real and synthetic. While synthetic datasets are utilized to assess the consistency in performance across real and synthetic images, real datasets are used to portray the level of detail and variation of actual blurred images. The dataset is divided into five categories (people, nature, manmade, text, and night light). Two image quality metrics were selected: full-reference assessment, including learned perceptual image patch similarity (LPIPS), peak signal-to-noise ratio (PSNR), and structural similarity indexing method (SSIM) for synthetic datasets, and no-reference assessments, including blind/reference-less image spatial quality (BRISQUE), natural image quality evaluator (NIQE) and perception-based image quality evaluator (PIQE) for real datasets. According to the findings, the fusion method performs best in the text category, followed by manmade and in nature, then night light and poor in people. The proposed method not only removes fine-scale edges and preserves the boundary sharpness, but also improved the estimated blur kernel.

1. Introduction

Photography is the art of creating images with a camera to keep for memories or future purposes. As new technology emerges, the field of photography is quickly progressing. Digital devices such as handheld cameras and smartphones make picture-taking more accessible, efficient, and cost-effective. However, image blurriness in uniform and non-uniform environments is an almost

* Corresponding author.

E-mail address: rechard@ums.edu.my

<https://doi.org/10.37934/araset.45.1.6070>

unavoidable issue when the object and the camera move differently during exposure. In most cases, retaking pictures is not an option as some moments cannot be recaptured under the same camera settings or in controlled situations [1]. Therefore, an image deblurring algorithm is proposed to obtain a sharper image from the blurred one taken in non-uniform environment.

Deblurring an image is a method that eliminates blurriness and improves image quality [2]. It has aided in the development of numerous applications, including picture segmentation, classification, and object recognition. Blind image deblurring, which estimates both the blur kernel and the latent picture, and non-blind image deblurring, which only estimates the latent image using the known kernel, are the two types of deblurring techniques. Blind image deblurring is commonly acknowledged to be a poorly stated problem because both the images and the blurring process information are lost [3].

Most of the existing algorithms for deblurring camera shake assume that the blurred image contains a spatially invariant filter and 2D convolution of a sharp image [4]. However, the camera shake in real life is more complex than simple 2-D translational motion, and it does not cause spatially-invariant blur [5]. Another issue to highlight is the presence of small-scale edges in the image. The estimated kernel will be less accurate when the images have strong but small-scale edges that introduce ambiguities [6]. Therefore, edges are essential when it comes to kernel estimation as it will lead to a better-estimated blur kernel with selected edges containing fewer saturated pixels [7]. In this study, non-blind motion deblurring using a single image and fine-scale edge removal will be mainly focused on deblurring and producing sharper quality results.

1.1 Related Works

In the early years, most deblurring methods focused on non-blind deconvolution methods such as Wiener Deconvolution and Richardson-Lucy algorithm. Weiner filtering is known for its simple computation and good restoration effect as it takes account of the degradation function and the statistical error function of noise [8]. Richardson-Lucy method is known for its implementation of maximum likelihood and ability to reconstruct good quality images in the presence of high noise levels [9]. Blind deconvolution is popularly known as an ill-posed problem due to the challenging estimation in both unknown blur kernel and latent image to reconstruct the blurred image to a sharper version [10].

A camera shake effect removal is proposed by applying natural image priors, and advanced statistical techniques with kernel estimation to match image camera motion [1]. However, ringing artifacts often happened near regions with high saturation and significant object motion, and they presumed that the cause of the artifacts was from the nonblind deconvolution step. A unified probabilistic model of blind and non-blind deconvolution is presented for motion deblurring purposes. An advanced iterative optimization alternates between blur kernel refinement and image restoration until convergence was used to solve the corresponding Maximum a Posteriori (MAP) problem [11].

Then, a two-phase kernel estimation method for single-image motion deblurring is suggested. Iterative support detection (ISD) optimization is used to refine the blur kernel once it is initially approximated using the selected image edges. The latent sharp image is then recovered via total-variation (TV)-1 deconvolution, followed by the imposition of a Gaussian prior to aid in the estimation of the blur kernel. Different motion assumptions, such as in-plane camera rotation or camera forward motion, have been used to represent the blur kernel [6].

A new type of image regularization based on normalized sparsity measure has been proposed to deblur both spatially invariant and spatially variant blur images. Unlike other existing models, this

model favours sharp images over blurry ones. In addition, the resulting scheme is quick since it used the existing fast $L1$ methods to estimate the kernel and sharp image [12].

Based on the observation that the dark channel of the blurred image is less sparse, the $L0$ -regularization term is used to enforce the sparsity of the latent image's dark channel, and an optimization algorithm based on a half-quadratic splitting strategy and look-up tables is proposed to restore the images regularised by the dark channel prior. If there are no dark pixels in the clear image, the dark channel cannot produce better results. Additionally, this approach assumes that just the blurring process alters the sparsity of the dark channel and that noise may have an impact on an image's dark pixels [13]. As discussed in [14] the magnitude of image structure was significantly reduced by motion blur led to imprecise kernel estimation. In [15] suggests that extending the $L0$ -regularization to non-uniform image deblurring with a better non-blind deconvolution approach.

Over the last few years, many neural network approaches have recently begun to be applied to image restoration algorithms. Estimating and removing non-uniform motion blur has been solved using a deep learning approach, a convolutional neural network (CNN). CNN is used to predict the probabilistic of different motion kernels for each image patch, whereas the Markov random field (MRF) model is adapted to estimate dense motion blur kernels for the whole image. With the advantage of the robust feature learning power of CNNs, the challenging non-uniform motion blur can be predicted [16]. And in [17] the author proposed unsupervised non blind deconvolution without the need to train with ground truth data. [18] introduces an end-to-end learning technique based on a conditional generative adversarial network (cGAN) and a multi-component loss function. This approach can keep texture details and is five times faster than previous work utilizing CNN.

2. Methodology

This study proposed an integrated deblurring algorithm (IDeA) in two steps, first by combining $L0$ -regularized intensity and gradient prior, scale aware smoothing enhanced with bilateral filtering to remove fine-scale in an image, then deblur an image with kernel estimation, and non-blind image deconvolution as depicted in Figure 1. The method acquired blurred images of five (5) categories (people, nature, manmade, text, and night light) as input. The images will be converted into 350x350 JPG images before the image acquisition for faster computation.

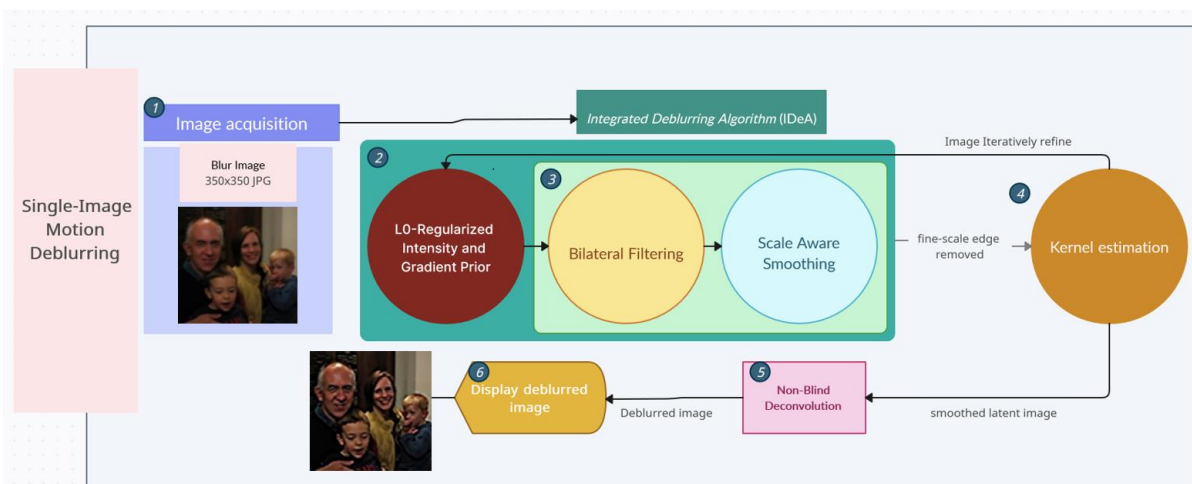


Fig. 1. Workflow of the proposed method

2.1 L_0 -Regularized Intensity and Gradient Prior

This method is based on intensity and gradient; thus, we use this method to model image gradients. Algorithm 1 illustrates the steps taken to implement the method.

Algorithm 1: L_0 regularized intensity and gradient prior	
Input: Blur image y and blur kernel k	
Output: Intermediate latent image x	
1.	$x \leftarrow y, \beta \leftarrow 2\lambda\sigma$
2.	repeat
3.	solve for u using
4.	$u = \begin{cases} x, & x ^2 \geq \frac{\lambda\sigma}{\beta} \\ 0, & \text{otherwise} \end{cases}$
5.	$u \leftarrow 2\lambda$
6.	repeat
7.	solve for g using
8.	$g = \begin{cases} \nabla x, & \nabla x ^2 \geq \frac{\lambda}{\mu} \\ 0, & \text{otherwise} \end{cases}$
9.	solve for x using
10.	$x = \mathcal{F}^{-1} \left(\frac{\overline{\mathcal{F}(k)}\mathcal{F}(y) + \beta\mathcal{F}(u) + \mu\mathcal{F}_G}{\overline{\mathcal{F}(k)}\mathcal{F}(k) + \beta + \mu\overline{\mathcal{F}(\nabla)}\mathcal{F}(\nabla)} \right)$
11.	$\mu \leftarrow 2\mu$
12.	until $\mu > \mu_{max}$
13.	$\beta \leftarrow 2\beta$
14.	until $\beta > \beta_{max}$

The image prior is defined as

$$P(x) = \sigma P_t(x) + P_t(\nabla x) \quad (1)$$

where σ (sigma) is the weight. The solution for Eq. (1) is obtained by alternatively solving

$$\min_x \|x * k - y\|_2^2 + \lambda P(x) \quad (2)$$

and

$$\min_k \|x * k - y\|_2^2 + \gamma \|k\|_2^2 \quad (3)$$

2.2 Fine-Scale Removal

At this stage, the intermediate latent image will first undergo bilateral filtering (in Algorithm 2) to remove small-scale edges, followed by L_0 Gradient Minimization to preserve the boundary sharpness.

Algorithm 2: Bilateral filtering

Input: Signal L , and parameters: w , σ_d , and σ_r
 Output: Smoothed edge image L'

1. $n = \text{length}(L)$
2. $L' = L$
3. for $i = \frac{w}{2} + 1$ to $\frac{w}{2} - 1$ do
4. $\text{GaussTemp} = e^{-\frac{(i-w)^2}{2\sigma_d^2}}$
5. end for
6. for $j = \frac{w}{2} + 1$ to $n - \frac{w}{2} + 1$ do
7. $\omega_1 = e^{-\frac{(L(j-\frac{w}{2}+1:j+\frac{w}{2}-1) - L(j))^2}{2\sigma_r^2}}$
8. $\omega_2 = \omega_1 * \text{GaussTemp}'$
9. $s = L(j - \frac{w}{2} + 1:j + \frac{w}{2} - 1) * \omega_2$
10. $L'(j) = \frac{\text{sum}(s)}{\text{sum}(\omega_2)}$
11. end for

At a pixel location $x = (x_1, x_2)$, the bilateral filter's output is computed as follows:

$$\hat{I}(x) = \frac{1}{C(x)} \sum_y K_d(\|y - x\|) K_r(|I(y) - I(x)|) I(y) \quad (4)$$

where $K_d(\cdot)$ is the spatial domain kernel, $K_r(\cdot)$ is the intensity range kernel, $N(x)$ is a spatial neighborhood of x , and $C(x)$ is the normalization constant:

$$C(x) = \sum_y K_d(\|y - x\|) K_r(|I(y) - I(x)|) \quad (5)$$

The kernel $K_d(\cdot)$ and $K_r(\cdot)$ determine how the spatial and intensity differences are treated. The contribution (weight) of a pixel $I(y)$ is determined by the product of $K_d(\cdot)$ and $K_r(\cdot)$. The most commonly used kernel is the Gaussian kernel, $G_\sigma(z) = \exp\left(\frac{-z^2}{2\sigma^2}\right)$, for both the domain and range kernels:

$$K_d(\|y - x\|) = G_{\sigma_d}(\|y - x\|) \quad (6)$$

and

$$K_r(|I(y) - I(x)|) = G_{\sigma_r}(|I(y) - I(x)|) \quad (7)$$

Both $K_d(\cdot)$ and $K_r(\cdot)$ use the Gaussian kernel, although the Sigma filter and the neighbourhood filter employ distinct kernels. The usage of outliers in calculating the spatial average is essentially eliminated by the sigma filter, which computes the local standard deviation σ around $I(x)$, and utilizes a threshold uniform box for the range kernel. For the neighborhood filter, the spatial kernel is a uniform box and the range kernel is Gaussian, as in Eq. (3).

After getting the smoothed image I_g , the L_0 gradient minimization computes the output smoothing result I_s by solving an objective function,

$$P(x) = \sigma P_t(x) + P_t(\nabla x) \quad (8)$$

where the data-fidelity term uses I_g and the regularization term uses I'_g . To prevent losing the image quality, the parameters are set as $\alpha = 1$, $\beta = 1.5$, and $\gamma = 0.5$ to make it more focused on luminance and contrast. For I'_g only gradient information is used for controlling the number of non-zero gradients. The parameters are set as $\alpha = 0.5$, $\beta = 1$, and $\gamma = 1.5$ to make it more focused on structure information and contrast.

2.3 Deblurring Images

With the given smoothed structural image x , the blur kernel k is estimated in the gradient space by

$$\min_k \|\nabla x * k - \nabla y\|_2^2 + \gamma \|k\|_2^2 \quad (9)$$

and FFTs are an effective method for computing the solution. The negative elements are set to 0 and normalized after obtaining k such that their sum equals 1. Kernel estimation is applied to estimate the blur kernel from the latent image. The initially blurred image y with blur kernel k is used to reconstruct a clearer image x . The cost function is given as:

$$\min_{x,w} \sum_i \left(\frac{\lambda}{2} (x \oplus k - y)_i^2 + \frac{\beta}{2} \left(\|F_i^1 x - w_i^1\|_2^2 + \|F_i^2 x - w_i^2\|_2^2 \right) + |w_i^1|^\alpha + |w_i^2|^\alpha \right) \quad (10)$$

where β is the weight that will vary during the optimization. Minimizing Eq. (10) for a fixed β can be performed by alternating between two steps, one where we solve for x , given values of w and vice-versa. Given a fixed value of w from the previous iteration, Eq. (10) is quadratic in x . The optimal x is:

$$\left(F^{1T} F^1 + F^{2T} F^2 + \frac{\lambda}{\beta} K^T K \right) x = F^{1T} w^1 + F^{2T} w^2 + \frac{\lambda}{\beta} K^T y \quad (11)$$

where $Kx \equiv x \oplus k$. Assuming circular boundary conditions, 2D FFT's which diagonalize the convolution matrices F^1, F^2, K is applied to find the optimal x directly:

$$x = \mathcal{F}^{-1} \left(\frac{\mathcal{F}(F^1)^* \circ \mathcal{F}(w^1) + \mathcal{F}(F^2)^* \circ \mathcal{F}(w^2) + (\lambda/\beta) \mathcal{F}(K)^* \circ \mathcal{F}(y)}{\mathcal{F}(F^1)^* \circ \mathcal{F}(F^1) + \mathcal{F}(F^2)^* \circ \mathcal{F}(F^2) + (\lambda/\beta) \mathcal{F}(K)^* \circ \mathcal{F}(K)} \right) \quad (12)$$

where $*$ are the complex conjugate and \circ denotes component-wise multiplication. The division is also performed component-wise. Solving Eq. (12) requires only 3 FFT's at each iteration since many of the terms can be precomputed. Given a fixed value of x , finding the optimal w consists of solving $2N$ independent 1D problems of the form:

$$w^* = \underset{w}{\operatorname{argmin}} |w|^\alpha + \frac{\beta}{2} (w - v)^2 \quad (13)$$

where $v \equiv F_i^j x$.

After the blur kernel is estimated, the blurred image and blur kernel will be fused to get a deblurred image.

2.4 Metrics and Data

Two image quality metrics to assess the proposed deblurring method performance were selected as presented in Table 1: full-reference (FR) assessment, including learned perceptual image patch similarity (LPIPS), peak signal-to-noise ratio (PSNR), and structural similarity indexing method (SSIM) for synthetic datasets [19], and no-reference (NR) assessments, including blind/reference-less image spatial quality (BRISQUE), natural image quality evaluator (NIQE) and perception-based image quality evaluator (PIQE) for real datasets [20].

Table 1
 Metrics descriptions

Metric	Class	Description
BRISQUE		
NIQE	NR	The lower the values, the better the image quality
PIQE		
LPIPS		The lower the value, the better the image quality
PSNR	FR	The larger the value, the more efficient the deblurring effect
SSIM		The closer the value to 1, is better

The input images used for the test are comprised of real and synthetic non-uniform datasets from previous study in [21] of five (5) categories (people, nature, manmade, text, and night light) as shown in Table 2. While synthetic datasets are utilized to assess the consistency in performance across real and synthetic images, real datasets are used to portray the level of detail and variation of actual blurred images.

Table 2
 Real and synthetic in the wild dataset

Sample No	Category	Real	Sample No	Synthetics
1	People		6	
2	Manmade		7	
3	Nature		8	
4	Text		9	
5	Night light		10	

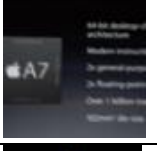
3. Results

The evaluation will be focusing on two aspects; the evaluation of fine-scale removal and the evaluation of the proposed single deblurring methods in each category based on visual perceptions and image quality metrics.

3.1 Fine-Scale Edge Removal Evaluation

As shown in Table 3, from the visual perception, the enhanced scale-aware smoothing successfully removes fine textures from the blurred image by smoothing the edge while preserving the structure of the image.

Table 3
 The output of real and synthetic datasets after deblurring

Sample No	Category	Real	Output	Sample No	Synthetics
1	People			6	 
2	Manmade			7	 
3	Nature			8	 
4	Text			9	 
5	Night light			10	 

Based on the SSIM results in Table 4, it is shown that all the values for both datasets are near 1, indicating small changes in flat regions. Hence, it can be concluded that the enhanced method effectively removes fine-scale edges.

Table 4
 Results for fine-scale removal on the real synthetic dataset

Real					
Sample No	1	2	3	4	5
SSIM	0.9890	0.9393	0.9518	0.9697	0.9659
Synthetics					
Sample No	6	7	8	9	10
SSIM	0.9445	0.9020	0.9218	0.9670	0.9439

3.1.1 Proposed IDeA evaluation

The reference images used in full-reference metrics for comparison are the original clear images. All the datasets will use the default parameter values with kernel size 41×41 for a fair comparison. The bolded values in all the tables indicate the best efficiency in deblurring and image quality. With the results obtained in each category, we can determine the optimal category for the proposed deblurring method. Table 5 to Table 9, shows the image quality metrics value obtained in each category.

As can be seen, the proposed method performs poorly in the people category. This not only shows in the quality metric but also in the visual output, where it overemphasizes the light region which gives an overexposure effect. We can say that the best performance is in the text category where the image is sharper and has less ringing effect around the text, followed by manmade and nature, then in night light. From the visual output in Table 3, although ringing artifacts and colour distortion can be found in manmade, nature, and night light images, the deblurred output is sharper and less blurry with a slightly ringing effect.

Table 5

Results for proposed IDeA on People category

Sample No	Type	Metric	Input	Proposed Method
1	Authentic	BRISQUE	32.88	46.45
		NIQE	16.45	21.38
		PIQE	22.15	58.17
6	Synthetic	LPIPS	0.2169	0.2767
		PSNR	68.10	63.01
		SSIM	0.6804	0.5556

Table 6

Results for proposed IDeA on Manmade category

Sample No	Type	Metric	Input	Proposed Method
2	Authentic	BRISQUE	32.09	26.33
		NIQE	28.79	19.19
		PIQE	6.89	26.48
7	Synthetic	LPIPS	0.3210	0.2226
		PSNR	60.87	57.23
		SSIM	0.3429	0.09589

Table 7

Results for proposed IDeA on Nature category

Sample No	Type	Metric	Input	Proposed Method
3	Authentic	BRISQUE	13.10	19.30
		NIQE	15.96	13.43
		PIQE	5.68	7.187
8	Synthetic	LPIPS	0.4939	0.3840
		PSNR	67.74	66.16
		SSIM	0.4973	0.4375

Table 8
Results for proposed IDeA on Text category

Sample No	Type	Metric	Input	Proposed Method
4	Authentic	BRISQUE	32.09	38.81
		NIQE	28.79	21.87
		PIQE	6.89	38.44
9	Synthetic	LPIPS	0.3210	0.1785
		PSNR	60.87	64.80
		SSIM	0.3429	0.7422

Table 9
Results for proposed IDeA on Night light category

Sample No	Type	Metric	Input	Proposed Method
5	Authentic	BRISQUE	13.10	9.028
		NIQE	15.96	16.25
		PIQE	5.68	5.934
10	Synthetic	LPIPS	0.4939	0.2795
		PSNR	67.74	61.82
		SSIM	0.4973	0.5158

4. Conclusions

An integrated single-image motion deblurring algorithm was proposed and put into practise in this research. Prior to image deblurring, regularised intensity, and gradient are applied before the improved scale-aware smoothing. Based on the SSIM metrics' assessment of the image quality of both real and synthetic images, it was determined that the goal to remove fine-scale edges had been accomplished. Each image's SSIM values are slightly different between blurred and smoothed images, as shown by the SSIM values in all of the images being close to 1. According to evaluation findings, the combination method performs best in the text category, followed by manmade and in nature, then night light and poor in people. However, more studies are needed to further improve the existing deblur method.

Acknowledgement

The author would like to express his appreciation and gratitude to the Research Management Centre, Universiti Malaysia Sabah for financial support in attending the 4th ICOAIMS 2023.

References

- [1] Fergus, Rob, Barun Singh, Aaron Hertzmann, Sam T. Roweis, and William T. Freeman. "Removing camera shake from a single photograph." In *Acm Siggraph 2006 Papers*, pp. 787-794. 2006. <https://doi.org/10.1145/1141911.1141956>
- [2] Sada, Mariya M., and M. G. Mahesh. "Image deblurring techniques—a detail review." *Int. J. Sci. Res. Sci. Eng. Technol* 4, no. 2 (2018): 15.
- [3] Xu, Xianqiu, Hongqing Liu, Yong Li, and Yi Zhou. "Image deblurring with blur kernel estimation in RGB channels." In *2016 IEEE international conference on digital signal processing (DSP)*, pp. 681-684. IEEE, 2016. <https://doi.org/10.1109/ICDSP.2016.7868645>
- [4] Cho, Sunghyun, and Seungyong Lee. "Fast motion deblurring." In *ACM SIGGRAPH Asia 2009 papers*, pp. 1-8. 2009. <https://doi.org/10.1145/1661412.1618491>
- [5] Levin, Anat, Yair Weiss, Fredo Durand, and William T. Freeman. "Understanding and evaluating blind deconvolution algorithms." In *2009 IEEE conference on computer vision and pattern recognition*, pp. 1964-1971. IEEE, 2009. <https://doi.org/10.1109/CVPRW.2009.5206815>

- [6] Xu, Li, and Jiaya Jia. "Two-phase kernel estimation for robust motion deblurring." In *Computer Vision—ECCV 2010: 11th European Conference on Computer Vision, Heraklion, Crete, Greece, September 5-11, 2010, Proceedings, Part I 11*, pp. 157-170. Springer Berlin Heidelberg, 2010. https://doi.org/10.1007/978-3-642-15549-9_12
- [7] Pan, Jinshan, Zhouchen Lin, Zhixun Su, and Ming-Hsuan Yang. "Robust kernel estimation with outliers handling for image deblurring." In *Proceedings of the IEEE Conference on Computer Vision and Pattern Recognition*, pp. 2800-2808. 2016. <https://doi.org/10.1109/CVPR.2016.306>
- [8] Wang, Yu-Kun, Fu-Ping Liu, Zhi-Peng Lu, Lei Guo, Shi-Ke Li, and Jian-Ping Pang. "Research on Image Restoration Algorithm for Blind Deconvolution." In *2018 4th Annual International Conference on Network and Information Systems for Computers (ICNISC)*, pp. 122-125. IEEE, 2018. <https://doi.org/10.1109/ICNISC.2018.00032>
- [9] Fish, D. A., A. M. Brinicombe, E. R. Pike, and J. G. Walker. "Blind deconvolution by means of the Richardson–Lucy algorithm." *JOSA A* 12, no. 1 (1995): 58-65. <https://doi.org/10.1364/JOSAA.12.000058>
- [10] Yu, XiaoYuan, and Wei Xie. "Single image blind deblurring based on salient edge-structures and elastic-net regularization." *Journal of Mathematical Imaging and Vision* 62 (2020): 1049-1061. <https://doi.org/10.1007/s10851-020-00949-6>
- [11] Shan, Qi, Jiaya Jia, and Aseem Agarwala. "High-quality motion deblurring from a single image." *Acm transactions on graphics (tog)* 27, no. 3 (2008): 1-10. <https://doi.org/10.1145/1360612.1360672>
- [12] Krishnan, Dilip, Terence Tay, and Rob Fergus. "Blind deconvolution using a normalized sparsity measure." In *CVPR 2011*, pp. 233-240. IEEE, 2011. <https://doi.org/10.1109/CVPR.2011.5995521>
- [13] Pan, Jinshan, Deqing Sun, Hanspeter Pfister, and Ming-Hsuan Yang. "Blind image deblurring using dark channel prior." In *Proceedings of the IEEE conference on computer vision and pattern recognition*, pp. 1628-1636. 2016. <https://doi.org/10.1109/CVPR.2016.180>
- [14] Qin, Fuqiang, Shuai Fang, Lifang Wang, Xiaohui Yuan, Mohamed Elhoseny, and Xiaojing Yuan. "Kernel learning for blind image recovery from motion blur." *Multimedia Tools and Applications* 79 (2020): 21873-21887. <https://doi.org/10.1007/s11042-020-09012-3>
- [15] Pan, Jinshan, Zhe Hu, Zhixun Su, and Ming-Hsuan Yang. "Deblurring text images via L0-regularized intensity and gradient prior." In *Proceedings of the IEEE Conference on Computer Vision and Pattern Recognition*, pp. 2901-2908. 2014. <https://doi.org/10.1109/CVPR.2014.371>
- [16] Sun, Jian, Wenfei Cao, Zongben Xu, and Jean Ponce. "Learning a convolutional neural network for non-uniform motion blur removal." In *Proceedings of the IEEE conference on computer vision and pattern recognition*, pp. 769-777. 2015. <https://doi.org/10.1109/CVPR.2015.7298677>
- [17] Quan, Yuhui, Zhuojie Chen, Huan Zheng, and Hui Ji. "Learning deep non-blind image deconvolution without ground truths." In *European Conference on Computer Vision*, pp. 642-659. Cham: Springer Nature Switzerland, 2022. https://doi.org/10.1007/978-3-031-20068-7_37
- [18] Kupyn, Orest, Volodymyr Budzan, Mykola Mykhailych, Dmytro Mishkin, and Jiří Matas. "Deblurgan: Blind motion deblurring using conditional adversarial networks." In *Proceedings of the IEEE conference on computer vision and pattern recognition*, pp. 8183-8192. 2018. <https://doi.org/10.1109/CVPR.2018.00854>
- [19] Razak, Muhammad Khairi A., Kamilah Abdullah, and Suhaila Abd Halim. "Non-blind Image Watermarking Algorithm based on Non-Separable Haar Wavelet Transform against Image Processing and Geometric Attacks." *Journal of Advanced Research in Applied Sciences and Engineering Technology* 29, no. 2 (2023): 251-267. <https://doi.org/10.37934/araset.29.2.251267>
- [20] Zhai, Guangtao, and Xiongkuo Min. "Perceptual image quality assessment: a survey." *Science China Information Sciences* 63 (2020): 1-52. <https://doi.org/10.1007/s11432-019-2757-1>
- [21] Lai, Wei-Sheng, Jia-Bin Huang, Zhe Hu, Narendra Ahuja, and Ming-Hsuan Yang. "A comparative study for single image blind deblurring." In *Proceedings of the IEEE Conference on Computer Vision and Pattern Recognition*, pp. 1701-1709. 2016. <https://doi.org/10.1109/CVPR.2016.188>